Robust Excitons and Trions in Monolayer $MoTe_2$

Jiong Yang,[†] Tieyu Lü,[‡,¥] Ye Win Myint,[†] Jiajie Pei,[†,§] Daniel Macdonald,[†] Jin-Cheng Zheng,[‡,¥] and Yuerui Lu*[,†]

[†]Research School of Engineering, College of Engineering and Computer Science, The Australian National University, Canberra, ACT, 0200, Australia, [‡]Department of Physics and Institute of Theoretical Physics and Astrophysics, Xiamen University, Xiamen, 361005, China, [¥]Department of Physics, and Fujian Provincial Key Laboratory of Theoretical and Computational Chemistry, Xiamen University, Xiamen, 361005, China, and [§]School of Mechanical Engineering, Beijing Institute of Technology, Beijing, 100081, China

ABSTRACT Molybdenum telluride ($MoTe_2$) has emerged as a special member in the family of two-dimensional transition metal dichalcogenide semiconductors, owing to the strong spin−orbit coupling and relatively small energy gap, which offers new applications in valleytronic and excitonic devices. Here we successfully demonstrated the electrical modulation of negatively charged (X^-), neutral (X^0), and positively charged (X^+) excitons in monolayer $MoTe_2$ *via* photoluminescence spectroscopy. The binding energies of X^+ and X^- were measured to be ~24 and ~27 meV, respectively. The exciton binding energy of monolayer $MoTe_2$ was measured to be 0.58 ± 0.08 eV *via* photoluminescence excitation spectroscopy, which matches well with our calculated value of 0.64 eV.

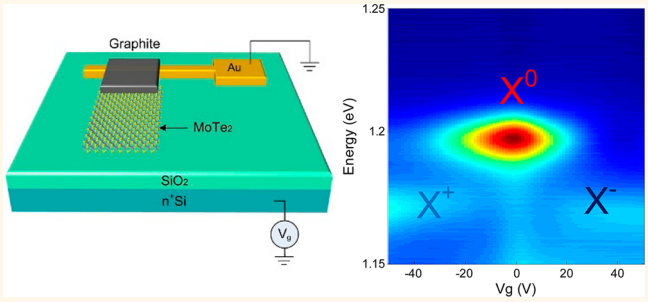

KEYWORDS: $MoTe_2$ · exciton · trion · two-dimensional

Atomically thin two-dimensional (2D) transition metal dichalcogenide (TMD) semiconductors have been of great interest, owing to their unique properties, such as enhanced Coulomb interactions arising from the reduced screening,[1,2] tightly bound excitons and trions (charged excitons),[3,4] strong interactions with light,[5−8] and so on. Much effort has been put into the investigations of neutral excitons and the positively or negatively charged excitons (trions) in 2D TMD semiconductors both experimentally[3,4,9−11] and theoretically.[12−15] Most of these studies have been focused on monolayer MX_2 (X = S, Se; M = Mo, W) TMD semiconductors. Very recently, 2H-$MoTe_2$ has arisen[16−21] as a special family member of 2D TMD semiconductors. The monolayer $MoTe_2$ consists of one hexagonal sheet of Mo atoms sandwiched between two hexagonal Te atoms with trigonal prismatic coordination. Multiple layers in the bulk crystal are bound together by van der Waals forces, and it can be easily exfoliated mechanically into monolayers. In contrast to other Mo-related TMD semiconductors MoX_2 (X = S, Se), $MoTe_2$ has a stronger spin−orbit coupling, which possibly leads to concomitantly longer decoherence time for exciton valley and spin indexes[18,22] and may enable new valleytronic devices.[23,24] The PL emission of $MoTe_2$ is located in the near-infrared range at around 1.1 eV,[16,17] bridging other comparatively large band-gap monolayer 2D TMD semiconductors and zero-band-gap graphene. Due to the small band gap, $MoTe_2$ is also considered an ideal system for studying exciton effects at the K point.[22,25] The exciton and trion peaks have been successfully observed in monolayer $MoTe_2$ under extremely low temperature (below 40 K).[16] But measurement of the exciton binding energy and the electrical modulation of exciton and trion dynamics in monolayer $MoTe_2$ are still lacking, which are very important for exploring new excitonic devices based on monolayer $MoTe_2$.

RESULTS AND DISCUSSION

In this paper, we demonstrated the electrical modulation of negatively charged (X^-), neutral (X^0), and positively charged (X^+) excitons *via* photoluminescence measurement

* Address correspondence to (Y. Lu) yuerui.lu@anu.edu.au.

Received for review May 4, 2015 and accepted June 3, 2015.

Published online June 03, 2015
10.1021/acsnano.5b02665

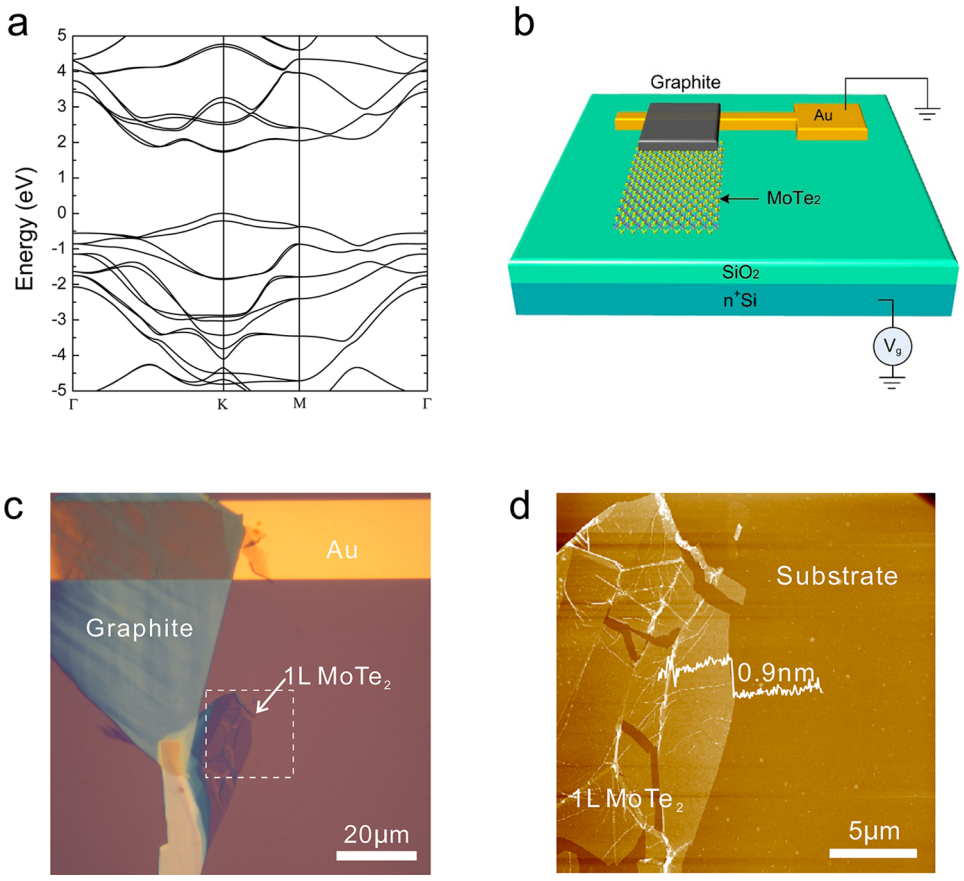

Figure 1. Calculated band diagram of monolayer (1L) $MoTe_2$ and the metal-oxide-semiconductor (MOS) structure. (a) Band diagram of 1L $MoTe_2$, indicating the direct band gap at the K point. (b) Schematic plot of a 1L $MoTe_2$ MOS device structure. Graphite is used as an electrical bridge. (c) Optical microscope image of the 1L $MoTe_2$ MOS device. (d) Atomic force microscopy (AFM) image of 1L $MoTe_2$ from the box enclosed by the dashed line in (c). The thickness from the height profile is 0.9 nm, well below the 2L thickness (~1.3 nm), indicating clearly that the sample is a monolayer.

on a monolayer $MoTe_2$ metal-oxide-semiconductor (MOS) device. The binding energies of X^+ and X^- were measured to be ~24 and ~27 meV, respectively. Moreover, the exciton binding energy of monolayer $MoTe_2$ was measured to be 0.58 ± 0.08 eV *via* photoluminescence excitation (PLE) spectroscopy, which matches well with our calculated value of 0.64 eV. Our work opens the door for the investigation of fundamental excitonic physics, as well as for a new generation of optoelectronic and excitonic devices based on monolayer $MoTe_2$.

First-principle calculations (Supporting Information Part I) based on density functional theory (DFT) have been performed, and the calculated band diagram of monolayer $MoTe_2$ is illustrated in Figure 1a, indicating that monolayer $MoTe_2$ is a direct band-gap semiconductor at the K point with a quasi-particle band gap of 1.72 eV, which agrees well with previous experiment[16,17] and calculations.[26] During the experiments, monolayer $MoTe_2$ was mechanically exfoliated from the bulk crystal purchased from HQ Graphene and dryly transferred[27] onto the SiO_2/Si (275 nm thermal oxide on n^+-doped silicon) substrate. The monolayer $MoTe_2$ was placed near a gold electrode that was prepatterned on the substrate. Another thick graphite flake was similarly transferred to electrically bridge the $MoTe_2$ flake and the gold electrode, forming a MOS device (Figure 1). This fabrication procedure kept the $MoTe_2$ free from chemical contaminations by minimizing the postprocesses after the $MoTe_2$ flake was transferred. In the measurement, the gold electrode is grounded, and the n^+-doped Si substrate functions as a back gate, providing uniform electrostatic doping in the $MoTe_2$ (Figure 1b). The optical microscope image of the MOS structure is shown in Figure 1c, with the AFM image shown in Figure 1d from the dashed line enclosed box in Figure 1c. The thickness from the atomic force microscopy (AFM) height profile is about 0.9 nm, well below the bilayer thickness of around 1.3−1.4 nm,[16,17] indicating clearly that this is a monolayer $MoTe_2$ sample.

After the sample preparation and characterization, electrical modulation was applied onto the monolayer $MoTe_2$ sample in order to investigate the exciton charging effects. All the PL measurements were conducted in a T64000 micro-Raman/PL system equipped with both a charge-coupled device (CCD) and InGaAs detectors, along with a 532 nm Nd:YAG laser as the

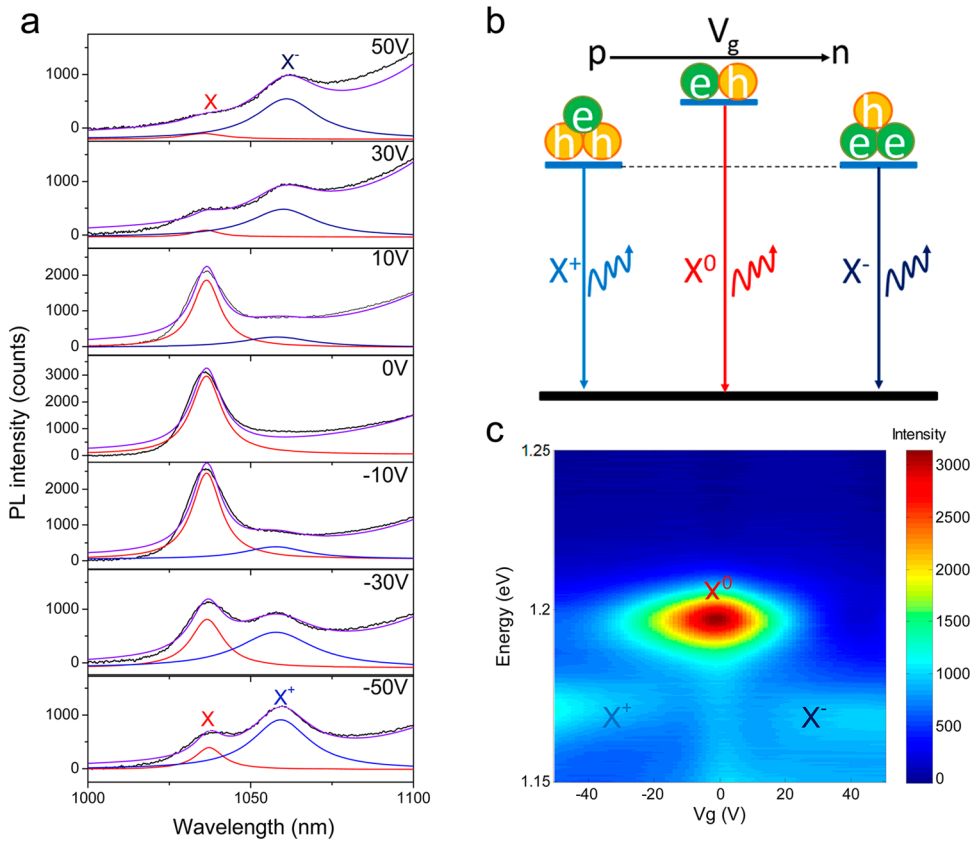

Figure 2. Electrical modulation of the exciton and trion dynamics for 1L $MoTe_2$. (a) Measured photoluminescence (PL) spectra of a 1L $MoTe_2$ sample at 83 K under different back gate voltages. Lorentzian fitting was used to extract the exciton and trion peaks of monolayer $MoTe_2$. Red and blue curves represent exciton and trion peaks of monolayer $MoTe_2$, respectively; black and purple curves are measured raw data and the cumulative fits. With nearly zero doping ($V_g = 0$ V), only neutral excitons can be observed, while with large electron (positive V_g)/hole (negative V_g) doping, negatively/positively charged excitons (trions) appear. (b) Schematic plot of the gate-dependent exciton and trion quasi-particle transitions. (c) The PL spectra of 1L $MoTe_2$ are plotted as a function of back gate voltage. The exciton, positive, and negative trion emissions are shown as bright spots in the 2D plot.

excitation source. Figure 2a displays the PL spectra at 83 K with a back gate voltage (V_g) from −50 to 50 V, and the black curve represents the original data from experiments. It is clear that, with zero electrical doping, only one sharp peak located at around 1035.6 nm (1.197 eV) can be observed. During our experiment, one broad peak located at around 1131.4 nm (1.096 eV) was also observed and was assigned to be the PL emission from n^+-doped Si (Figure S2), which is not our focus in this paper. With the increase of electron (negative V_g) or hole (positive V_g) doping, the sharp PL emission peak split into two peaks, locating separately at 1036.9 nm (1.196 eV) and 1057.8 nm (1.172 eV) for $V_g = -50$ V. Under positive voltage bias ($V_g > 0$), the energy difference between these two sharp peaks is a bit higher, which will be discussed further below. The intensity weight of these two peaks can be modulated by back gate voltage, and the peak with lower energy came to dominate with high doping level. Besides, the lower energy peaks appearing at both positive and negative V_g have similar energies. Taking into account previous research on charged excitons,[3,4] we assign the higher energy sharp peak as the neutral exciton peak (X^0) and the lower energy sharp peak as negatively or positively charged excitons (negative trions X^- or positive trions X^+) (Figure 2b and c). Lorentzian fitting is used to extract the exciton and trion peaks of monolayer $MoTe_2$. In Figure 2a, red and blue curves represent the exciton and trion peak of monolayer $MoTe_2$, respectively, with the purple curve as the cumulative fit. The schematic of the exciton and trion transition[4] with back gate modulation is displayed in Figure 2b. Electrons and holes are represented with green and yellow circles with *e* and *h* in the middle. The monolayer $MoTe_2$ sample is initially nearly undoped, and only neutral exciton emission can be detected. When applying positive back gate voltage, electrons will be injected into the monolayer $MoTe_2$, forming negatively charged excitons (or negative trions); likewise positively charged excitons (or positive trions) will form when holes are injected into the system with negative back gate voltage. This process can be represented as $e(h) + X^0 \rightarrow X^-(X^+)$. In order to have a better view of the exciton and trion transition, the PL spectra are plotted as a function of back gate voltage with measured PL

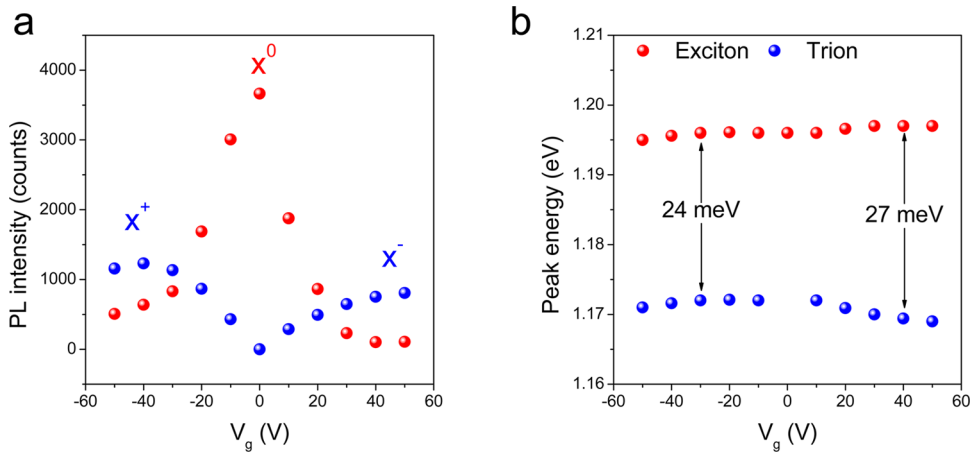

Figure 3. Exciton and trion analysis of 1L $MoTe_2$. (a) Exciton and trion peak intensities under different back gate voltages. (b) Exciton and trion peak energies under different back gate voltages. The binding energies of positive trion and negative trions are measured to be ~24 and ~27 meV, respectively.

intensity as a color scale, as indicated in Figure 2c. Only exciton and trion peaks of monolayer $MoTe_2$ are plotted here since the broad PL peak of Si is not our focus. We can clearly see the high-energy exciton bright spot (marked with X^0) when V_g is near 0 V, and when V_g increases or decreases, the exciton spot fades and the other two light spots show up (marked as X^- for positive V_g and X^+ for negative V_g), unambiguously indicating the exiciton and trion transition with external electrical doping.

To further analyze the exciton and trion transition dynamics in the monolayer $MoTe_2$ system, exciton and trion PL intensities are plotted in Figure 3a. The intensity of the exciton peak reaches its maximum when V_g = 0 V and gradually drops to almost zero when the sample is either positively or negatively doped under high-voltage bias, V_g, while the intensity of the trion peak is zero when V_g = 0 V and saturates when the sample is either positively or negatively doped under high-voltage bias, V_g (*i.e.*, ±50 V). The integrated PL intensity from the exciton peak (at V_g = 0 V) is about twice those from the trion peaks (at V_g = ±50 V) (Figure S3), which might be caused by the different internal quantum efficiency of these different emission types.[28] The exciton and trion peak energies from the fitting curves are plotted in Figure 3b. We found that the binding energy of positive and negative trions, *i.e.*, the peak energy difference of exciton and trion peaks, varies by about 3 meV, with the positive trion binding energy being ~24 meV and negative trion binding energy ~27 meV. The difference between the binding energies of positive and negative trions might be related to the different carrier density, dielectric screening, and effective masses of carriers in monolayer $MoTe_2$.[3,12,15]

The direct measurement of the exciton binding energy of monolayer $MoTe_2$ is also very important for the fundamental studies of many-body interactions and for the exploration of new optoelectronic devices. Here, photoluminescence excitation measurements were conducted to determine the exciton binding energy of monolayer $MoTe_2$ at room temperature. The sample used in the PLE measurements was on a transparent gel film and was the same piece for the electric modulation test previously transferred onto the Si/SiO_2 substrate, with the microscope image shown in Figure S4. In the experiments, the excitation wavelength was swept from 990 nm to 510 nm (1.25−2.43 eV) with a supercontinuum laser (SuperK EXTREME) with a precalibrated constant laser power of 40 μW. The experimental results are plotted in Figure 4a as a 2D plot, with the *x*-axis as the emission photon energy and the *y*-axis as the excitation photon energy. Figure 4b displays three PL spectra with excitation wavelengths of 590, 690, and 730 nm (2.10, 1.80, and 1.70 eV; black, red, and green curve, respectively) along the corresponding color dashed lines in Figure 4a. From Figure 4a and b, it is clear to see that the PL intensity reaches its maximum with the excitation wavelength of 690 nm, while the emission peak is located at the same energy level since the PL emission is mainly from the same excitons. In Figure 4c, the PL peak intensity is extracted along the white dashed line in Figure 4a and presented as a function of the exciton energy. The PL peak intensity first increases and then decreases with the increase of the excitation energy, with a PL intensity maximum at the excitation energy of 1.80 eV.

To further understand why the PL intensity reaches its maximum at the excitation energy of 1.80 eV, a first-principle calculation was performed of the absorption as a function of photon energy, and the results are presented in the lower panel of Figure 4d. The red and blue curves represent the calculation results with and without considering the electron−hole interactions, respectively. The experimental results are presented in the upper panel, with the narrow red band as the exciton peak energy and the broad blue band as

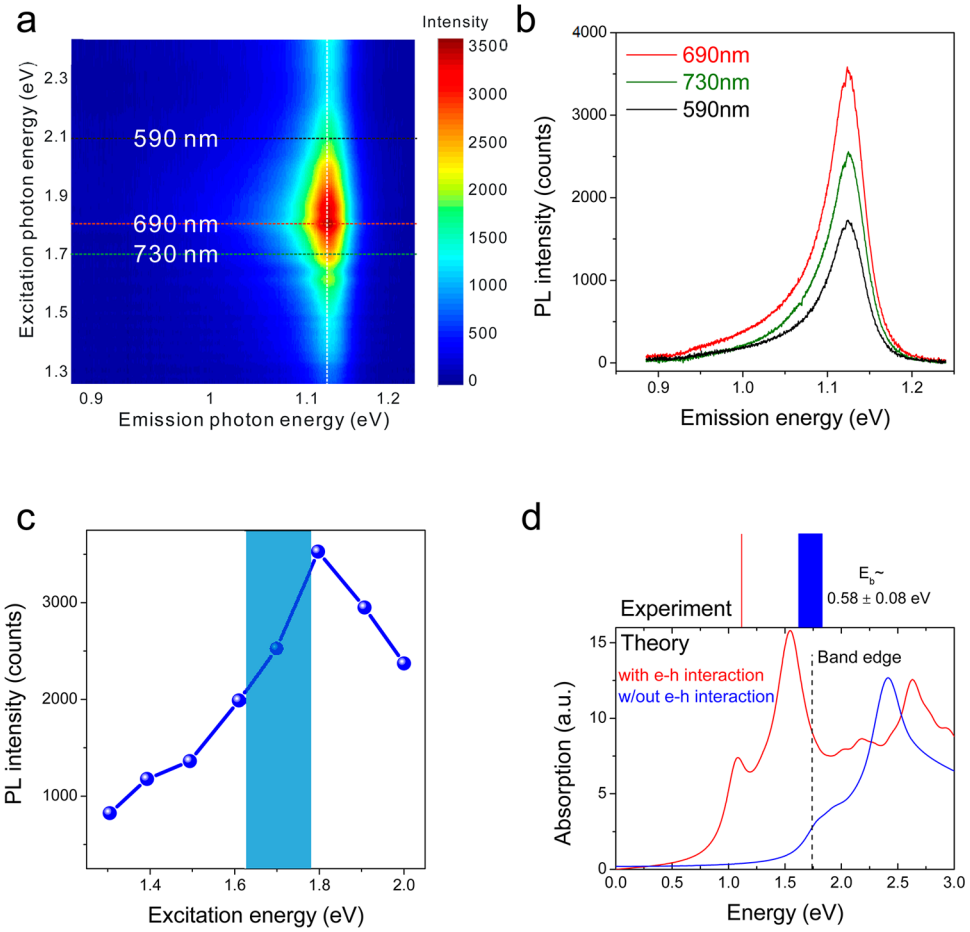

Figure 4. Photoluminescence excitation (PLE) spectra of 1L $MoTe_2$. (a) PLE intensity map of 1L $MoTe_2$ on a transparent gel film, measured at room temperature. (b) Selected PL spectra along the three horizontal dashed lines indicated in (a), showing that the PL becomes strongest when the excitation energy is at 1.80 eV (690 nm). (c) PL intensity at the emission peak of 1.12 eV as a function of excitation photon energy. The data are taken along the vertical dashed line in (a). (d) Upper: Schematic of measured exciton energy (narrow red band) and the energy of the quasi-particle band edge (broad blue band). The width of the bands indicates the experimental uncertainty. Lower: Absorption spectra from calculation with the *e*−*h* interaction (excitonic, red curve) and without the *e*−*h* interaction (quasi-particle, blue curve).

the quasi-particle band edge and the width of these two bands representing the experimental uncertainty. From our experiments, the exciton emission peak is located at 1.12 eV, matching well with the theoretical calculation. Also, the quasi-particle band edge extracted from the light blue band in Figure 4c is 1.70 ± 0.08 eV, matching reasonably well with the calculated band edge, indicated by a vertical dashed line in Figure 4d, where the band edge is defined as the point where the PL emission has the maximum increase rate.[29] This measured and calculated band edge at ~1.7 eV corresponds well with the measured absorption peak at ~1.8 eV from reflectance contrast $\Delta R/R$ spectra by Ruppet *et al.*[17] Ruppet *et al.*[17] have measured the reflectance contrast $\Delta R/R$ spectra for mono-, bi-, and trilayer $MoTe_2$ crystals on the SiO_2 substrate and successfully observed the *A* and *B*, *A*′ and *B*′, and *C* and *D* absorption peaks. *A* and *B* peaks are assigned to excitonic peaks associated with the lowest direct optical transition at the K point. The splitting between the *A*, *B* and *A*′, *B*′ has been related to interlayer interactions since they are only observed in bi- and trilayer $MoTe_2$ samples, and *C* and *D* peaks are attributed to regions of parallel bands near the Γ point, which corresponds to the band nesting effect reported by Kozawa *et al.*[30] For the monolayer $MoTe_2$ sample, Ruppet *et al.* observed an absorption peak at ~1.8 eV, and they did not explain the origin of this peak. This value is quite consistent with both our measured absorption peak from PLE measurements and theoretical calculations, and we attribute the absorption peak at ~1.8 eV to the band edge. Hence from our experiments, the exciton binding energy of monolayer $MoTe_2$ is 0.58 ± 0.08 eV, which matches well with our calculated value of 0.64 eV. This measured exciton binding energy of monolayer $MoTe_2$ is comparable with those of other 2D TMD semiconductors.[30]

CONCLUSIONS

In conclusion, we have successfully demonstrated the electrical modulation of excitons and trions in monolayer $MoTe_2$. Both positive and negative trions

have been observed with electrostatic doping in a MOS device. The extracted binding energies of positive and negative trions were ~24 and ~27 meV, respectively. Furthermore, the exciton binding energy of monolayer $MoTe_2$ was determined to be 0.58 ± 0.08 eV *via* PLE spectroscopy measurements, consistent with our first-principle calculation result of 0.64 eV. Our research and experimental results here pave the way for future applications in near-infrared optoelectronic and excitonic devices with this material.

EXPERIMENTAL METHODS

The monolayer $MoTe_2$ sample was transferred onto a SiO_2/Si substrate (275 nm thermal SiO_2) by mechanical exfoliation, using GEL film (Gel-Pak). The monolayer $MoTe_2$ was placed near a gold electrode that was prepatterned on the substrate. Another thick graphite flake was similarly transferred to electrically bridge the $MoTe_2$ flake and the gold electrode, forming a MOS device. This fabrication procedure kept the $MoTe_2$ free from chemical contaminations by minimizing the postprocesses after the $MoTe_2$ flake was transferred. In the measurement, the gold electrode is grounded, and the n^+-doped Si substrate functions as a back gate, providing uniform electrostatic doping in the $MoTe_2$. All PL measurements were conducted with a T64000 micro-Raman system equipped with both CCD and InGaAs detectors. Photoluminescence excitation measurements were conducted to determine the exciton binding energy of monolayer $MoTe_2$ at room temperature. The sample used in the PLE measurements was on a transparent gel film and was the same piece for the electric modulation test previously transferred onto the Si/SiO_2 substrate.

Conflict of Interest: The authors declare no competing financial interest.

Acknowledgment. We would like to thank Prof. Chennupati Jagadish and Prof. Barry Luther-Davies from The Australian National University for their facility support. We acknowledge financial support from an ANU Ph.D. student scholarship, China Scholarship Council, Australian Research Council (grant no. DE140100805), and ANU Major Equipment Committee (grant no. 14MEC34). T.Y.L. and J.C.Z. acknowledge the support of the National Science Foundation of China (grant no. U1232110).

Supporting Information Available: Details of theoretical calculation methods, more experimental PL measurement results, and data analysis. The Supporting Information is available free of charge on the ACS Publications website at DOI: 10.1021/acsnano.5b02665.

REFERENCES AND NOTES

1. Chernikov, A.; Berkelbach, T. C.; Hill, H. M.; Rigosi, A.; Li, Y.; Aslan, O. B.; Reichman, D. R.; Hybertsen, M. S.; Heinz, T. F. Exciton Binding Energy and Nonhydrogenic Rydberg Series in Monolayer WS_2. *Phys. Rev. Lett.* **2014**, *113*, 076802.
2. Ugeda, M. M.; Bradley, A. J.; Shi, S.-F.; da Jornada, F. H.; Zhang, Y.; Qiu, D. Y.; Ruan, W.; Mo, S.-K.; Hussain, Z.; Shen, Z.-X.; *et al*. Giant Bandgap Renormalization and Excitonic Effects in a Monolayer Transition Metal Dichalcogenide Semiconductor. *Nat. Mater.* **2014**, *13*, 1091–1095.
3. Mak, K. F.; He, K.; Lee, C.; Lee, G. H.; Hone, J.; Heinz, T. F.; Shan, J. Tightly Bound Trions in Monolayer MoS_2. *Nat. Mater.* **2013**, *12*, 207–211.
4. Ross, J. S.; Wu, S.; Yu, H.; Ghimire, N. J.; Jones, A. M.; Aivazian, G.; Yan, J.; Mandrus, D. G.; Xiao, D.; Yao, W.; *et al*. Electrical Control of Neutral and Charged Excitons in a Monolayer Semiconductor. *Nat. Commun.* **2013**, *4*, 1474.
5. Britnell, L.; Ribeiro, R. M.; Eckmann, A.; Jalil, R.; Belle, B. D.; Mishchenko, A.; Kim, Y.-J.; Gorbachev, R. V.; Georgiou, T.; Morozov, S. V.; *et al*. Strong Light-Matter Interactions in Heterostructures of Atomically Thin Films. *Science* **2013**, *340*, 1311–1314.
6. Eda, G.; Maier, S. A. Two-Dimensional Crystals: Managing Light for Optoelectronics. *ACS Nano* **2013**, *7*, 5660–5665.
7. Yang, J.; Wang, Z.; Wang, F.; Xu, R.; Tao, J.; Zhang, S.; Qin, Q.; Luther-Davies, B.; Jagadish, C.; Yu, Z., *et al*. *Atomically Thin Optical Lenses and Gratings*. *arXiv:1411.6200*, **2014**.
8. Tsai, M.-L.; Su, S.-H.; Chang, J.-K.; Tsai, D.-S.; Chen, C.-H.; Wu, C.-I.; Li, L.-J.; Chen, L.-J.; He, J.-H. Monolayer MoS_2 Heterojunction Solar Cells. *ACS Nano* **2014**, *8*, 8317–8322.
9. Ross, J. S.; Klement, P.; Jones, A. M.; Ghimire, N. J.; Yan, J.; Mandrus, D. G.; Taniguchi, T.; Watanabe, K.; Kitamura, K.; Yao, W.; *et al*. Electrically Tunable Excitonic Light-Emitting Diodes Based on Monolayer Wse2 P-N Junctions. *Nat. Nanotechnol.* **2014**, *9*, 268–272.
10. Hill, H. M.; Rigosi, A. F.; Roquelet, C.; Chernikov, A.; Berkelbach, T. C.; Reichman, D. R.; Hybertsen, M. S.; Brus, L. E.; Heinz, T. F. Observation of Excitonic Rydberg States in Monolayer MoS_2 and WS_2 by Photoluminescence Excitation Spectroscopy. *Nano Lett.* **2015**, *15*, 2992–2997.
11. Zhu, B.; Chen, X.; Cui, X. Exciton Binding Energy of Monolayer Ws2. *Sci. Rep.* **2015**, *5*.
12. Ganchev, B.; Drummond, N.; Aleiner, I.; Fal'ko, V. Three-Particle Complexes in Two-Dimensional Semiconductors. *Phys. Rev. Lett.* **2015**, *114*, 107401.
13. Thilagam, A. Exciton Complexes in Low Dimensional Transition Metal Dichalcogenides. *J. Appl. Phys.* **2014**, *116*, 053523.
14. Berkelbach, T. C.; Hybertsen, M. S.; Reichman, D. R. Theory of Neutral and Charged Excitons in Monolayer Transition Metal Dichalcogenides. *Phys. Rev. B* **2013**, *88*, 045318.
15. Thilagam, A. Two-Dimensional Charged-Exciton Complexes. *Phys. Rev. B* **1997**, *55*, 7804–7808.
16. Lezama, I. G.; Arora, A.; Ubaldini, A.; Barreteau, C.; Giannini, E.; Potemski, M.; Morpurgo, A. F. Indirect-to-Direct Band Gap Crossover in Few-Layer $MoTe_2$. *Nano Lett.* **2015**, *15*, 2336–2342.
17. Ruppert, C.; Aslan, O. B.; Heinz, T. F. Optical Properties and Band Gap of Single- and Few-Layer $MoTe_2$ Crystals. *Nano Lett.* **2014**, *14*, 6231–6236.
18. Pradhan, N. R.; Rhodes, D.; Feng, S.; Xin, Y.; Memaran, S.; Moon, B.-H.; Terrones, H.; Terrones, M.; Balicas, L. Field-Effect Transistors Based on Few-Layered A- $MoTe_2$. *ACS Nano* **2014**, *8*, 5911–5920.
19. Yamamoto, M.; Wang, S. T.; Ni, M.; Lin, Y.-F.; Li, S.-L.; Aikawa, S.; Jian, W.-B.; Ueno, K.; Wakabayashi, K.; Tsukagoshi, K. Strong Enhancement of Raman Scattering from a Bulk-Inactive Vibrational Mode in Few-Layer $MoTe_2$. *ACS Nano* **2014**, *8*, 3895–3903.
20. Lezama, I. G.; Ubaldini, A.; Longobardi, M.; Giannini, E.; Renner, C.; Kuzmenko, A. B.; Morpurgo, A. F. Surface Transport and Band Gap Structure of Exfoliated 2h- $MoTe_2$ Crystals. *2D Mater.* **2014**, *1*, 021002.
21. Fathipour, S.; Ma, N.; Hwang, W. S.; Protasenko, V.; Vishwanath, S.; Xing, H. G.; Xu, H.; Jena, D.; Appenzeller, J.; Seabaugh, A. Exfoliated Multilayer $MoTe_2$ Field-Effect Transistors. *Appl. Phys. Lett.* **2014**, *105*, 192101.
22. Guo, H.; Yang, T.; Yamamoto, M.; Zhou, L.; Ishikawa, R.; Ueno, K.; Tsukagoshi, K.; Zhang, Z.; Dresselhaus, M. S.; Saito, R. *Double Resonance Raman Modes in Mono- and Few-Layer $MoTe_2$*. *arXiv:1501.07078*, **2015**.
23. Mai, C.; Barrette, A.; Yu, Y.; Semenov, Y. G.; Kim, K. W.; Cao, L.; Gundogdu, K. Many-Body Effects in Valleytronics: Direct Measurement of Valley Lifetimes in Single-Layer MoS_2. *Nano Lett.* **2013**, *14*, 202–206.
24. Urbaszek, B.; Marie, X. Valleytronics: Divide and Polarize. *Nat. Phys.* **2015**, *11*, 94–95.
25. Wilson, J. A.; Yoffe, A. D. The Transition Metal Dichalcogenides Discussion and Interpretation of the Observed

Optical, Electrical and Structural Properties. *Adv. Phys.* **1969**, *18*, 193–335.
26. Ramasubramaniam, A. Large Excitonic Effects in Monolayers of Molybdenum and Tungsten Dichalcogenides. *Phys. Rev. B* **2012**, *86*, 115409.
27. Castellanos-Gomez, A.; Buscema, M.; Molenaar, R.; Singh, V.; Janssen, L.; Zant, H. S. J. v. d.; Steele, G. A. Deterministic Transfer of Two-Dimensional Materials by All-Dry Viscoelastic Stamping. *2D Mater.* **2014**, *1*, 011002.
28. Galland, C.; Ghosh, Y.; Steinbruck, A.; Sykora, M.; Hollingsworth, J. A.; Klimov, V. I.; Htoon, H. Two Types of Luminescence Blinking Revealed by Spectroelectrochemistry of Single Quantum Dots. *Nature* **2011**, *479*, 203–207.
29. Wang, X.; Jones, A. M.; Seyler, K. L.; Tran, V.; Jia, Y.; Zhao, H.; Wang, H.; Yang, L.; Xu, X.; Xia, A. F. *Highly Anisotropic and Robust Excitons in Monolayer Black Phosphorus*. *preprint arXiv:1411.1695*, **2014**.
30. Kozawa, D.; Kumar, R.; Carvalho, A.; Kumar Amara, K.; Zhao, W.; Wang, S.; Toh, M.; Ribeiro, R. M.; Castro Neto, A. H.; Matsuda, K.; *et al*. Photocarrier Relaxation Pathway in Two-Dimensional Semiconducting Transition Metal Dichalcogenides. *Nat. Commun.* **2014**, *5*, 4543.